
FraGNNet: A Deep Probabilistic Model for Mass Spectrum Prediction

Adamo Young^{*123} Fei Wang^{*45} David Wishart⁴⁶⁷⁸ Bo Wang¹²⁹¹⁰ Hannes Röst¹¹³ Russ Greiner⁴⁵

Abstract

The process of identifying a compound from its mass spectrum is a critical step in the analysis of complex mixtures. Typical solutions for the mass spectrum to compound (MS2C) problem involve matching the unknown spectrum against a library of known spectrum-molecule pairs, an approach that is limited by incomplete library coverage. Compound to mass spectrum (C2MS) models can improve retrieval rates by augmenting real libraries with predicted spectra. Unfortunately, many existing C2MS models suffer from problems with prediction resolution, scalability, or interpretability. We develop a new probabilistic method for C2MS prediction, FraGNNet, that can efficiently and accurately predict high-resolution spectra. FraGNNet uses a structured latent space to provide insight into the underlying processes that define the spectrum. Our model achieves state-of-the-art performance in terms of prediction error, and surpasses existing C2MS models as a tool for retrieval-based MS2C.

1. Introduction

Small molecule identification from complex mixtures is a challenging problem with far-reaching implications. Determining the chemical composition of a liquid sample is a

^{*}Equal contribution ¹Department of Computer Science, University of Toronto, Toronto, Canada ²Vector Institute for Artificial Intelligence, Toronto, Canada ³Terrence Donnelly Centre for Cellular and Biomolecular Research, University of Toronto, Toronto, Canada ⁴Department of Computing Science, University of Alberta, Edmonton, Canada ⁵Alberta Machine Intelligence Institute, Edmonton, Canada ⁶Department of Biological Sciences, University of Alberta, Edmonton, Alberta ⁷Department of Laboratory Medicine and Pathology, University of Alberta, Edmonton, Alberta ⁸Faculty of Pharmacy and Pharmaceutical Sciences, University of Alberta, Edmonton, Alberta ⁹Department of Laboratory Medicine and Pathobiology, University of Toronto, Toronto, Canada ¹⁰Peter Munk Cardiac Centre, University Health Network, Toronto Canada ¹¹Department of Molecular Genetics, University of Toronto, Toronto, Canada. Correspondence to: Hannes Röst <hannes.rost@utoronto.ca>, Russ Greiner <rgreiner@ualberta.ca>.

critical step not only in the discovery of novel compounds but also in the recognition of known compounds within new contexts. Tandem mass spectrometry (MS/MS) is a widely employed tool for molecule identification, with applications ranking from drug discovery to environmental science to metabolism research (Dueñas et al., 2022; Gowda & Djukovic, 2014; Peters, 2011; Lebedev, 2013). Analyzing the set of MS/MS spectra measured from a liquid sample (such as human blood or plant extract) can reveal important information about its constitution.

The mass spectrum to compound (MS2C) problem refers to the task of identifying a molecule from its mass spectrum. Existing MS2C workflows often rely on comparing the spectrum of an unknown molecule against a library of reference spectra with known identities. However, spectral libraries are far from comprehensive, so *retrieval-based* MS2C might not work even for molecules that are otherwise well-characterized.

Many computational approaches attack the MS2C problem head-on by attempting to predict structural features of the molecule directly from the spectrum. Some models infer high-level chemical properties from the spectrum (Dührkop et al., 2015; Voronov et al., 2022) and use these features to recommend likely candidate structures from existing chemical databases (Dührkop et al., 2015; Dührkop et al., 2019; Goldman et al., 2023b;c) or guide generative models towards potential matches (Stravs et al., 2022). Other methods formulate the problem as sequence-to-sequence translation (Butler et al., 2023; Shrivastava et al., 2021) and attempt to predict a string representation of the structure from the spectrum.

Compound to mass spectrum (C2MS) prediction can be viewed as an indirect approach for solving the MS2C problem. Instead of attempting to infer structural features from the spectrum, C2MS models work by boosting the effectiveness of existing retrieval-based MS2C workflows. Accurate C2MS models can predict spectra for millions of molecules that are missing from spectral libraries, improving coverage by orders of magnitude. This kind of library augmentation has been a mainstay in retrieval-based MS2C workflows for over a decade (Wolf et al., 2010; Allen et al., 2015; Wishart et al., 2018) and has led to the successful identification of novel compounds (Skinnider et al., 2021; Wang et al.,

Arxiv preprint. Copyright 2024 by the author(s).

2023).

Despite numerous advances, challenges with MS2C remain (Schymanski et al., 2017), motivating the development of better C2MS models. Ideally, mass spectra should be predicted at a high resolution, to avoid loss of information. The prediction model itself must be reasonably fast, so that large-scale library generation for MS2C is feasible. Finally, model predictions should be interpretable enough to facilitate manual validation of MS2C identifications.

In this work, we make the following contributions:

- We introduce FraGNNNet, a novel method for mass spectrum prediction that integrates combinatorial bond-breaking methods with principled probabilistic modelling.
- We argue that this approach meets key requirements in the areas of resolution, scalability, and interpretability.
- Through comparisons with strong baseline models, we demonstrate that FraGNNNet achieves state-of-the-art performance on spectrum prediction and compound retrieval tasks.

2. Background

At a high level, tandem mass spectrometry provides information about a molecule’s structure by measuring how it fragments. The experimental process is outlined in Figure 1. First, molecules in the sample are ionized: at this stage they are referred to as *precursor ions*, because they have not yet undergone fragmentation. In liquid samples, each molecule may become associated with a charged *adduct* during ionization. For example, if the adduct is a hydrogen ion H^+ , an $[M+H]^+$ precursor ion will form. Following ionization, the mass to charge ratio (m/z) of each precursor ion is subsequently measured using a mass analyzer. After the precursor m/z values are recorded, ions with a particular m/z are selected for further analysis in the form of fragmentation. The fragmentation process is typically facilitated by energetic collisions with neutral gas particles, and can be influenced by experimental parameters such as *collision energy*.

After fragmentation, the resulting charged ions are sent back to the mass analyzer for m/z measurement, producing a distribution over fragment m/z values that reflects how often each fragment was formed. Often there are multiple fragments with nearly identical m/z , complicating analysis of the spectrum. Since the fragmentation process is stochastic, an individual precursor ion can break down into different fragments with different probabilities. However, with a sufficiently high precursor ion concentration, enough independent fragmentations can occur such that sampling error is no longer a concern. The mass spectrum

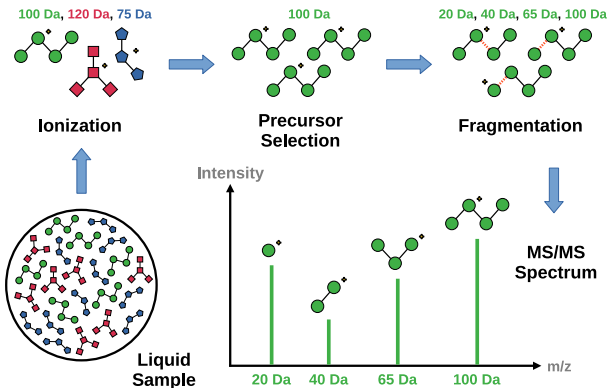


Figure 1. Overview of MS/MS: molecules in the sample are ionized to form precursors, filtered by precursor m/z (100 Da), and sent for fragmentation. The fragmentation process stochastically produces fragments with m/z values of 20, 40, 65 Da. The distribution of precursor and fragment m/z values forms the spectrum.

is defined as the probability distribution over the fragment m/z values. Since the charge z is usually $+1$ or -1 for small molecules, the spectrum can also be interpreted as a distribution over masses, where each mass is measured in Daltons (Da). Throughout this work, we focus our analysis on $[M+H]^+$ spectra (where z is always $+1$), although our methods can easily be extended to other types of precursor ions.

The process of fragmentation involves breakage and formation of bonds between atoms in the molecule. Each fragment is, by definition, composed of a subset of the atoms in the original precursor. Fragmentation is typically modelled as a sequence of high-energy reactions. Generally, a reaction involves a charged fragment (which could be the precursor) being converted into two sub-fragments, only one of which is charged. The neutral (uncharged) sub-fragment is described as a *neutral loss* because it cannot be measured by the mass spectrometer and ends up getting discarded. The charged sub-fragment may undergo further reactions to produce additional fragments. The most common type of reaction is an α -Cleavage, which results in the removal of a single bond. More complicated reactions are possible (McLafferty, 1959; Biemann, 1962; van Tetering et al., 2024), but in many cases these reactions can be approximated as sequences of bond breakages.

Mathematically, a mass spectrum Y can be represented as a finite set of tuples $\{(m_j, P(m_j))\}_j$ where each mass m_j has an associated probability $P(m_j)$. Individual tuples $(m_j, P(m_j))$ are often referred to as *peaks*, with the mass m_j being called the *peak location* and the probability $P(m_j)$ being called the *peak intensity*. The problem of spectrum prediction can be formulated as a standard supervised learning task. The dataset is composed of N tuples $\{(X_i, Y_i)\}_{i=1}^N$ where X_i is a molecule and Y_i is its asso-

ciated mass spectrum. The set of masses in a particular spectrum Y_i is denoted as M_i . The goal of a C2MS model is to predict Y_i from X_i .

3. Related Work

The increasing availability of small molecule MS/MS data has led to a proliferation of machine learning models for spectrum prediction. Existing methods can be broadly grouped into two categories, *binned* and *structured*, based on how they represent the spectrum.

Binned methods approximate the spectrum as a sequence of discrete mass bins with associated peak intensities. This reduces the spectrum prediction problem to a vector regression task, which can be readily solved without extensive domain-specific model customization. Binned approaches generally vary based on the strategy they employ for encoding the input molecule: multi-layer perceptrons (Wei et al., 2019), 2D (Zhu et al., 2020; Li et al., 2022) and 3D (Hong et al., 2023) graph neural networks, and graph transformers (Young et al., 2023) have all been used successfully. However, selecting an appropriate bin size can be challenging: bins that are too large result in loss of information, while bins that are too small can be overly sensitive to measurement error and yield high-dimensional spectrum vectors that are impractical to model. This presents a fundamental roadblock for the application of binned models in retrieval-based MS2C.

Structured approaches sidestep the binning problem by modelling the spectrum as a distribution over chemical formulae, whose masses can be calculated trivially with extremely high precision. Some methods predict the formula distribution directly, using either autoregressive formula generation (Goldman et al., 2023a) or a large fixed formula vocabulary (Murphy et al., 2023). Others rely on recursive fragmentation (Wang et al., 2021; Zhu & Jonas, 2023) or autoregressive generation (Goldman et al., 2024) to model a distribution over fragments, which induces a distribution over formulae. While structured MS2C models can generate very high resolution spectra, they tend to be slower than binned approaches due to the increased complexity of the output space.

There is a natural trade-off between a model’s scalability and the amount of information it can provide about the fragmentation process. Methods that infer fragment distributions are most informative, since they explicitly describe how the molecule breaks apart. However, these models tend to involve stronger priors and more complex prediction schemes (Wang et al., 2021; Zhu & Jonas, 2023; Goldman et al., 2024) to facilitate efficient exploration of the combinatorial fragment space. FraGNNNet takes a pragmatic approach, achieving a level of interpretability that approaches that of

the most sophisticated fragmentation models, while maintaining high performance and scalability (see Appendix C).

4. Methods

4.1. Overview

The goal of our method is to predict a high resolution MS/MS spectrum based on an input molecular structure. The model works in two stages: first, a heuristic bond-breaking algorithm (Section 4.2) generates a set of plausible molecule fragments. Then, a probabilistic model (Section 4.3) parameterized by a graph neural network (Section 4.4) predicts a distribution over these fragments. The fragment distribution induces a distribution over chemical formulae, which is converted to a mass spectrum by mapping formula masses. This approach allows for extremely high resolution peak predictions with built-in formula and fragment annotations.

4.2. Recursive Fragmentation

A small organic molecule can be represented as an undirected graph $G = (V, E)$. Each node $a \in V$ represents an atom in the molecule with an associated element label $\omega_a \in \Omega$ (where $\Omega = \{C, H, N, O, P, S, \dots\}$ is a finite set of common elements) and each edge $b \in E$ represents a covalent bond between atoms. Let $S(G)$ be the set of connected subgraphs of the graph G .

Definition 4.1. The graph $\mathcal{F}(G) = (\mathcal{F}_1(V), \mathcal{F}_2(E))$ is called a fragmentation DAG with respect to the graph G if the following properties hold:

1. Each node $n \in \mathcal{F}_1(V)$ maps to a connected subgraph $G_n \in S(G)$
2. A directed edge $e \in \mathcal{F}_2(E)$ from node $u \in \mathcal{F}_1(V)$ to node $v \in \mathcal{F}_1(V)$ can exist if and only if $G_v \in S(G)$ is a connected subgraph of $G_u \in S(G)$.

Note that the root node r of $\mathcal{F}(G)$ always maps to the original graph G , and the leaves of $\mathcal{F}(G)$ correspond to individual atoms $a \in V$.

Most fragments in a mass spectrum can be modelled as products of a series of bond breakages. Such fragments will thus appear as nodes $n \in \mathcal{F}_1(V)$, and their fragmentation history can be represented as a path from the root r to n . It is possible to derive a set of chemical formulae $F(\mathcal{F}(G)) = \{f_n : n \in \mathcal{F}_1(V)\}$, where each formula f_n is a $|\Omega|$ -dimensional vector representing the element counts of atoms in G_n . This set $F(\mathcal{F}(G))$ can be used to calculate the set of possible peak locations in the spectrum, $M(G) = \{m_n : n \in \mathcal{F}_1(V)\}$ where $m_n = \text{mass}(f_n)$ is the mass of formula f_n .

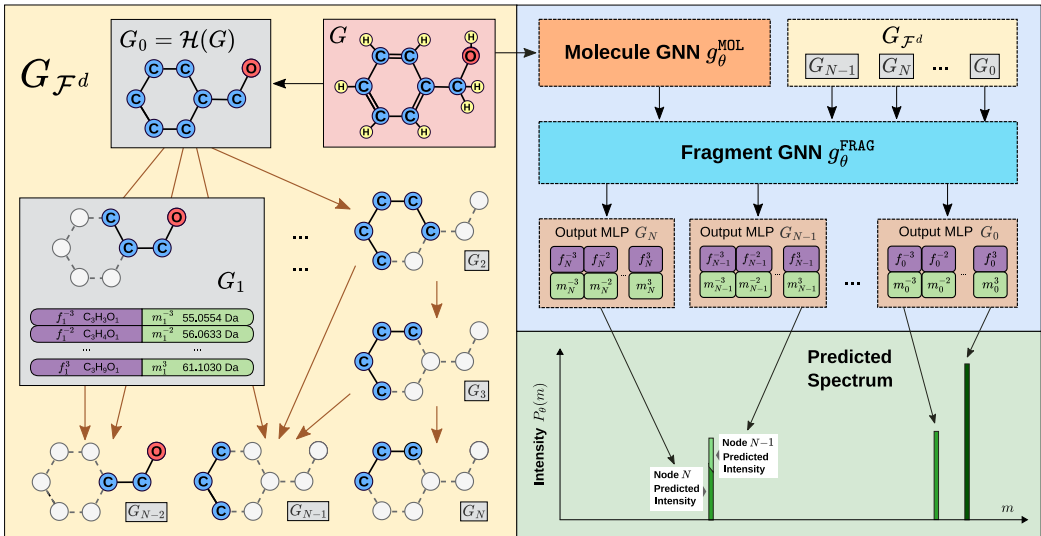


Figure 2. Overview of the FraGNNNet C2MS model. The input molecule (G , red box) is processed into an approximate Fragmentation DAG ($G_{\mathcal{F}^d}$, yellow box) and independently embedded by the Molecule GNN (g_{θ}^{MOL} , orange box). Information from the DAG is combined with the molecule embedding and processed by the Fragment GNN (g_{θ}^{FRAG} , blue box). Output MLPs (brown boxes) are applied to each fragment node n in the DAG to predict a per-node distribution over formulae (purple boxes), which can be mapped to a distribution over masses (green boxes) and summed across nodes to create the MS/MS spectrum.

The fragmentation DAG $\mathcal{F}(G)$ can be a useful tool for spectrum prediction (Wang et al., 2021; Goldman et al., 2023a; 2024), providing information about peak locations and relationships between fragments in the spectrum. However, computing $\mathcal{F}(G)$ from G through exhaustive edge removal can be expensive, requiring on the order of $\mathcal{O}(2^{|E|})$ operations. Inspired by previous approaches from the literature (Wolf et al., 2010; Ruttkies et al., 2016; Allen et al., 2015; Ridder et al., 2014; Goldman et al., 2024), we approximate $\mathcal{F}(G)$ using a few simplifying assumptions.

Definition 4.2. The graph $\mathcal{H}(G) = (\mathcal{H}_1(V), \mathcal{H}_2(E))$ is called a heavy atom skeleton of G if $\mathcal{H}(G)$ is the largest connected subgraph of G such that $\omega_a \neq \text{H}$ (hydrogen) for all $a \in \mathcal{H}_1(V)$.

Since $|\mathcal{H}_2(E)|$ is often smaller than $|E|$ by a factor of 2-3, calculating $\mathcal{F}(\mathcal{H}(G))$ is considerably faster than calculating $\mathcal{F}(G)$. We employ a recursive edge removal (i.e. bond-breaking) algorithm that only considers nodes that are at most d hops away from the root r , producing a connected subgraph $\mathcal{F}^d(\mathcal{H}(G))$.

For simplicity of notation, we refer to $\mathcal{F}^d(\mathcal{H}(G))$ as $G_{\mathcal{F}^d}$, with vertex set $V_{\mathcal{F}^d}$ and edge set $E_{\mathcal{F}^d}$. Since, by definition, each node $n \in V_{\mathcal{F}^d}$ corresponds to a subgraph $G_n \in \mathcal{S}(G)$ that does not contain any hydrogen atoms, we employ a heuristic to model the possible number of hydrogens associated with each G_n . Let h_n be the number of hydrogen atoms in G that are connected to the subgraph G_n . We define the set $\{h_n - j, \dots, h_n + j\}$ as the range of hydrogen counts for the subgraph G_n , where j is a tolerance parameter.

This induces a set of possible formulae $\{f_n^{-j}, \dots, f_n^j\}$ and associated masses $\{m_n^{-j}, \dots, m_n^j\}$, where f_n^i is a formula with the same heavy atom counts as f_n and $h_n + i$ hydrogens, and m_n^i is its corresponding mass. Hydrogen transfers are common in fragmentation, so allowing for flexibility in the hydrogen counts can result in a more representative set of formulae.

Definition 4.3. The set

$$\hat{M}(G, d, j) = \bigcup_{n \in V_{\mathcal{F}^d}} \{m_n^{-j}, \dots, m_n^j\}$$

is the set of masses derived from the approximate heavy-atom fragmentation DAG $G_{\mathcal{F}^d}$ with hydrogen tolerance j .

Empirically, we find that calculating $\hat{M}(G, d, j)$ (Definition 4.3) with $d \in \{3, 4\}$ and $j = 4$ can effectively capture most of the total peak intensity in real MS data (see Appendix B).

4.3. Probabilistic Formulation

Our model can be interpreted as a structured latent variable model whose latent distributions depend on a molecular graph G and its approximate fragmentation DAG $G_{\mathcal{F}^d}$.

To begin, we define the following latent probability distributions:

Definition 4.4. Let $P_{\theta}(n)$ be a discrete finite probability distribution over the DAG nodes $n \in V_{\mathcal{F}^d}$, parameterized by a neural network g_{θ} .

Definition 4.5. Let $P_{\theta}(f|n)$ be a discrete finite conditional

distribution between DAG nodes $n \in V_{\mathcal{F}^d}$ and associated formulae $\{f_n^{-j}, \dots, f_n^j\}$, parameterized by a neural network g_θ .

Both distributions depend implicitly on the molecular graph G , but for clarity of notation we have omitted this. Note that for each node n , $P_\theta(f|n)$ has support over $2j+1$ formulae.¹

The joint distribution $P_\theta(n, f) = P_\theta(n) P_\theta(f|n)$ can be loosely interpreted as identifying which substructures are generated during fragmentation, with $P_\theta(n)$ modelling the heavy atom structures of the probable fragments and $P_\theta(f|n)$ identifying the number of hydrogens associated with each of those fragments.

By marginalizing $P_\theta(n, f)$ over the nodes n , it is possible to calculate a distribution over formulae $P_\theta(f)$. Since each formula f has an associated mass, the discrete distribution $P_\theta(f)$ can be easily converted to a continuous distribution $P_\theta(m)$ over masses. Following (Allen et al., 2015), we formulate $P_\theta(m)$ as a mixture of univariate Gaussians as outlined in Equation 1:

$$\begin{aligned} P_\theta(m) &= \sum_f P_\theta(f) P(m|f) \\ &= \sum_f P_\theta(f) \mathcal{N}(\mu(f), \sigma(f)) \end{aligned} \quad (1)$$

The conditional $P(m|f)$ is a narrow truncated Gaussian centered on the formula mass, $\mu(f) = \text{mass}(f)$, with variance $\sigma(f)$ proportional to f and truncation occurring at ± 1 standard deviation from the mean. This Gaussian model approximates the typical error distribution of the mass analyzer (Allen et al., 2015). At inference time it is convenient to approximate $P(m)$ as a discrete distribution with $P(m|f) = \delta(\text{mass}(f))$, where δ is the Dirac delta function.

It is possible to calculate another distribution $P_\theta(n|f)$ using Bayes Theorem. Intuitively $P_\theta(n|f)$ identifies which fragments n are contributing to a predicted peak centered at formula f – for this reason we refer to it as the *peak annotation distribution*. While not directly used to generate the spectrum, $P_\theta(n|f)$ can be helpful for interpreting model behaviour (see Section 5.3, Figure 3).

In Appendix D, we describe alternate versions of $P_\theta(n)$, $P_\theta(f|n)$, and $P_\theta(n|f)$ that account for fragment subgraph isomorphism.

4.4. Neural Network Parameterization

The distributions $P_\theta(n)$ and $P_\theta(f|n)$ are parameterized by a two-stage graph neural network (GNN, Battaglia et al. 2018) as defined by Equation 2:

$$g_\theta(G, G_{\mathcal{F}^d}) = g_\theta^{\text{FRAG}}(g_\theta^{\text{MOL}}(G), G_{\mathcal{F}^d}) \quad (2)$$

The first stage g_θ^{MOL} , called the *Molecule GNN*, operates on the input molecular graph G . The second stage g_θ^{FRAG} , called the *Fragment GNN*, combines information from the fragmentation DAG and the molecule embeddings to predict the distributions $P_\theta(n)$ and $P_\theta(f|n)$.

4.4.1. MOLECULE GNN

The Molecule GNN g_θ^{MOL} takes the input molecular graph G and outputs embeddings for the atoms in the graph. The atom embeddings $\bar{h}_a^{(0)}$ and bond embeddings $\bar{h}_b^{(0)}$ are initialized with specific features from G (see Appendix E).

GNN models work by iteratively updating node states through the aggregation of neighbourhood information. g_θ^{MOL} uses the GINE architecture (Xu et al., 2018; Fey & Lenssen, 2019), which incorporates both node and edge information in its updates. The GINE update rule is given by equation 3, where l is the GNN layer index, $l \in \{1, \dots, L_1\}$, and g_θ is a standard multi-layer perceptron (MLP):

$$\bar{h}_a^{(l+1)} = g_\theta \left(\bar{h}_a^{(l)} + \sum_{u \in \mathbb{N}(a)} \text{ReLU}(\bar{h}_u^{(l)} + \bar{h}_b^{(l)}) \right) \quad (3)$$

The final atom embeddings $\bar{h}_a^{(L_1)}$ are subsequently passed to the Fragment GNN g_θ^{FRAG} for further processing.

4.4.2. FRAGMENT GNN

The Fragment GNN g_θ^{FRAG} is another GINE network that propagates information along the approximate fragmentation DAG. Each DAG node $n \in V_{\mathcal{F}^d}$ is featurized using information about its associated subgraph G_n , precisely described in Equations 4 and 5. The vector $\bar{h}_n^{(0)}$ is a concatenation of three terms: \hat{h}_n^s is the average atom embedding for atoms in G_n ; \hat{h}_n^f is an embedding of the subgraph formula f_n ; and \hat{h}_n^d is an embedding of the depth in the DAG at which node n is located.

$$\bar{h}_n^{(0)} = \hat{h}_n^s \parallel \hat{h}_n^f \parallel \hat{h}_n^d \quad (4)$$

$$\hat{h}_n^s = \frac{1}{|V_n|} \sum_{a \in V_n} \bar{h}_a^{(L_1)} \quad (5)$$

The edge embeddings $\bar{h}_e^{(0)}$ are also initialized with subgraph information: they capture differences between adjacent DAG nodes. Refer to Appendix F for full details.

The DAG nodes are processed by the Fragment GNN in a manner that is similar to Equation 3. After L_2 layers of processing, a small output MLP is applied to each node

¹There is additional filtering for chemical validity which may mask out some formulae, but for clarity this has been omitted.

embedding $\bar{h}_n^{(L_2)}$, producing a $2j + 1$ dimensional vector representing the unnormalized logits for $P_\theta(n, f_n^i)$ for each $i \in \{-j, \dots, j\}$. The other latent distributions in Section 4.3 are calculated from the joint through normalization, marginalization, and application of Bayes Theorem.

While performing model ablations (see Appendix H), we discovered that edge information could be omitted without degradation in performance, allowing for 2x faster training and inference. As a result, the experiments in Section 5 use a variant of g_θ^{FRAG} that excludes the neighbourhood aggregation term from the GINE update.

4.5. Loss Function

We fit the parameters of the model θ with maximum likelihood estimation, using stochastic gradient descent. The loss function is based on the negative log-likelihood of the data, defined in Equation 6:

$$\mathcal{L}_{\text{NLL}}(\theta) = \frac{1}{N} \sum_{i=1}^N \sum_{m \in M_i} -P_i(m) \log P_\theta(m) \quad (6)$$

For each spectrum, a subset of the peak masses $M_i^{\text{OS}} \subseteq M_i$ are defined to be *Outside of the Support (OS)* if they are far enough from away the predicted set of masses $\hat{M}(G_i, d, j)$ such that their predicted probability is 0 (Equation 7). The rest of the masses $M_i^{\text{IS}} = M_i - M_i^{\text{OS}}$ are deemed to be *Inside of the Support (IS)*.

$$P_i(M_i^{\text{OS}}) = \sum_{m \in M_i: P_\theta(m)=0} P_i(m) \quad (7)$$

Modelling the OS probability can provide useful information about the reliability of the predicted spectrum. With slight modification, FraGNNNet can be adapted to predict $P_\theta(M_i^{\text{OS}})$, an estimation of $P_i(M_i^{\text{OS}})$. Adjusting the loss function $\mathcal{L}_{\text{NLL}}(\theta)$ to incorporate an OS cross-entropy term yields Equation 8:

$$\mathcal{L}(\theta) = \frac{1}{N} \sum_{i=1}^N \sum_{m \in M_i^{\text{IS}}} -P_i(m) \log P_\theta(m) - P_i(M_i^{\text{OS}}) \log P_\theta(M_i^{\text{OS}}) \quad (8)$$

In cases where $P_i(M_i^{\text{OS}}) > 0$, perfectly optimizing $\mathcal{L}_{\text{NLL}}(\theta)$ yields predictions which have (incorrectly) redistributed $P_i(M_i^{\text{OS}})$ to other peaks. This undesirable behaviour can be avoided by minimizing $\mathcal{L}(\theta)$ instead.

4.6. Latent Entropy Regularization

Latent entropies can provide insight into the model’s understanding of the fragmentation process. $H_\theta(n)$ describes the diversity of fragment skeletons that were generated; $H_\theta(f|n)$ describes variability in hydrogen configurations

for each skeleton; $H_\theta(n|f)$ describes variability in peak annotations.

Since entropy is differentiable, joint optimization of latent entropy and prediction error is possible using gradient-based methods. The normalized entropy $\hat{H}(x) = H(x)/\log(|X|)$ is preferable for optimization since it accounts for differences in latent support size caused by variations in the size of the input molecule. Incorporating normalized entropy into the objective function, as demonstrated in Equation 9, effectively imposes entropy regularization on the latent distributions:

$$\begin{aligned} \mathcal{L}_{\text{REG}}(\theta) &= \mathcal{L}(\theta) \\ &+ \alpha_n \hat{H}_\theta(n) + \alpha_f \hat{H}_\theta(f) \\ &+ \alpha_{f|n} \hat{H}_\theta(f|n) + \alpha_{n|f} \hat{H}_\theta(n|f) \end{aligned} \quad (9)$$

The tunable hyperparameters $\{\alpha_n, \alpha_f, \alpha_{f|n}, \alpha_{n|f}\}$ control the influence of the entropy regularizers. Since $\mathcal{L}_{\text{REG}}(\theta)$ is minimized, setting $\alpha_x < 0$ will maximize the corresponding normalized entropy $\hat{H}_\theta(x)$, and vice versa. Entropy regularization can be useful when assessing consistency of peak annotations, as demonstrated in Section 5.3.

5. Experiments

5.1. Spectrum Prediction (C2MS)

FraGNNNet’s C2MS performance is evaluated on a held-out portion of the NIST20 MS/MS dataset (Appendix I), to allow for comparison with other binned and structured prediction models from the literature.

ICEBERG (Goldman et al., 2024) is a structured method for high-resolution spectrum prediction that uses a two-stage model. The first stage autoregressively predicts a set of fragments, and the second stage predicts a mapping between those fragments and the peaks in the spectrum (see Appendix C). The stages are trained independently, with the first stage approximating the output of a heuristic fragmenter, MAGMa (Ridder et al., 2014), that uses signals from the spectrum to find a minimal set of fragments that explain the peaks. We introduce ICEBERG-ADV (advanced), a variant of ICEBERG that replaces the first stage of the model with the exact MAGMa output. This modification removes sampling error in the fragment generation process, creating an artificially easier learning problem that should result in better performance. We emphasize that ICEBERG-ADV is only suitable for benchmarking: in most realistic C2MS problems ground truth spectra are not available at inference time, meaning that MAGMa cannot be applied.

The other baseline models, MassFormer (Young et al., 2023) and NEIMS (Wei et al., 2019), both predict binned spectra at

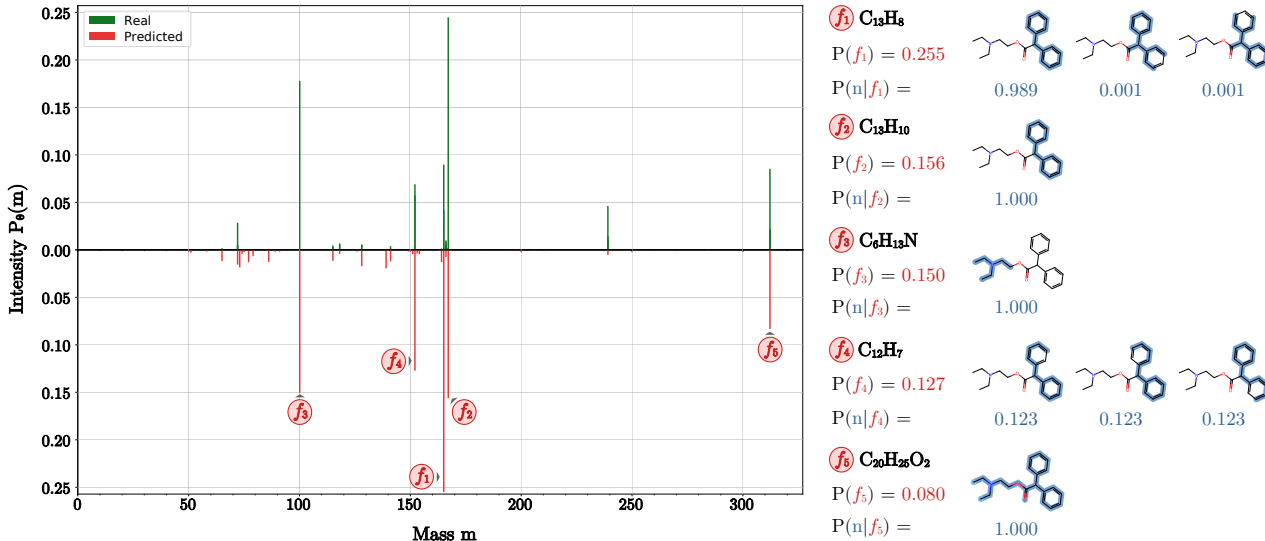


Figure 3. Example Spectrum Prediction with Fragment Annotations: A real spectrum (green) for a molecule from the test set, Adiphenine, is compared with its corresponding FraGNNNet-D4 prediction (red). The five most intense peak predictions are annotated with formulae and up to three probable fragment structures. The structure annotation for peak 5 clearly corresponds to the precursor ion (i.e. the entire graph). The model is uncertain about the annotation for peak 4, giving equal probability to related structures.

a lower resolution. The former uses a pretrained graph transformer model (Ying et al., 2021) to encode the molecule, while the latter relies on domain-specific chemical fingerprint representations (Rogers & Hahn, 2010).

The results are summarized in Table 1. FraGNNNet-D4, a version of our model that uses a $d = 4$ approximation of the fragmentation DAG, clearly outperforms other models in terms of cosine similarity. The binned spectrum approaches (NEIMS and MassFormer) score much worse in terms of cosine hungarian similarity (Appendix G) due to the limited resolution afforded by their binned spectrum representation.

Increasing fragmentation depth from $d = 3$ to $d = 4$ seems to have a positive impact on performance. Lower $P(M^{OS})$ with FraGNNNet-D4 is indicative of better mass coverage when compared to FraGNNNet-D3, leading to better similarity scores. Both models are able to estimate $P(M^{OS})$ to some degree, suggesting that FraGNNNet can identify situations *at inference time* where its fragmentation model will be inaccurate.

5.2. Compound Retrieval (MS2C)

FraGNNNet was also evaluated in a retrieval-based MS2C task. Our setup is similar to previous methods (Goldman et al., 2024; Murphy et al., 2023): for each (X_i, Y_i) in the NIST20 Test set (roughly 4000 pairs, Appendix I) a candidate set C_i is constructed from X_i and 49 other compounds sampled from PubChem (Kim et al., 2019). Each $C_i \in C_i - \{X_i\}$ is selected to have high chemical similarity with X_i as measured by Tanimoto similarity between chem-

ical fingerprints (Rogers & Hahn, 2010). The C2MS models are tasked with predicting a set of spectra \hat{Y}_i for molecules $C_i \in C_i$. The spectra \hat{Y}_i are ranked by their cosine hungarian similarity (Appendix G) with the real spectrum Y_i , inducing a ranking on the molecules C_i . The models are scored based on their ability to correctly rank X_i in the Top- k for $k \in \{1, 3, 5, 10\}$. FraGNNNet outperform all baseline models for for all values of k (see Tables 2 and 8).

5.3. Annotation Consistency

When interpreting mass spectral data, practitioners will annotate each peak in the spectrum with a substructure to explain what happened during fragmentation. FraGNNNet’s latent distribution $P_\theta(n|f)$ provides a map from formulae f to DAG nodes n and their associated subgraphs G_n . $P_\theta(n|f)$ can be interpreted as a peak annotation distribution (see Figure 3 for an example), with the mode $\arg \max_n P_\theta(n|f)$ identifying the subgraph that contributes most to the peak located at $\text{mass}(f)$.

It is difficult to evaluate the correctness of peak annotations (human-derived or otherwise) without additional experimental analysis (van Tetering et al., 2024). However, we can measure the *consistency* of annotations across models that perform equally well. Inter-model differences in latent distributions that do not affect overall C2MS performance are indicative of ambiguity in the fragmentation process. Similar to how ensembles can be used to estimate prediction uncertainty (Lakshminarayanan et al., 2017), identifying annotation inconsistencies across a group of models with

Table 1. Spectrum Prediction Performance on the NIST20 Dataset. Means and standard deviations are reported for 5 random seeds, with best scores in bold. As NEIMS and MassFormer are binned models, they cannot be scored with COS_{HUN} and have no notion of $P(M^{OS})$. ICEBERG and ICEBERG-ADV do not predict $P_\theta(M^{OS})$ so they cannot be scored with $|P(M^{OS}) - P_\theta(M^{OS})|$.

SPLIT	MODEL	$COS_{0.01} \uparrow$	$COS_{HUN} \uparrow$	$P(M^{OS}) \downarrow$	$ P(M^{OS}) - P_\theta(M^{OS}) \downarrow$
INCHIKEY	FRAGNET-D4	0.717 ± 0.001	0.691 ± 0.001	0.097 ± 0.000	0.053 ± 0.002
INCHIKEY	FRAGNET-D3	0.702 ± 0.002	0.675 ± 0.001	0.171 ± 0.000	0.078 ± 0.001
INCHIKEY	ICEBERG-ADV	0.702 ± 0.002	0.666 ± 0.002	0.158 ± 0.000	-
INCHIKEY	ICEBERG	0.681 ± 0.002	0.645 ± 0.002	0.178 ± 0.000	-
INCHIKEY	MASSFORMER	0.653 ± 0.003	-	-	-
INCHIKEY	NEIMS	0.642 ± 0.001	-	-	-
SCAFFOLD	FRAGNET-D4	0.654 ± 0.003	0.630 ± 0.004	0.109 ± 0.000	0.063 ± 0.001
SCAFFOLD	FRAGNET-D3	0.637 ± 0.003	0.612 ± 0.003	0.192 ± 0.000	0.095 ± 0.002
SCAFFOLD	ICEBERG-ADV	0.643 ± 0.002	0.611 ± 0.002	0.175 ± 0.000	-
SCAFFOLD	ICEBERG	0.618 ± 0.001	0.586 ± 0.001	0.200 ± 0.000	-
SCAFFOLD	MASSFORMER	0.600 ± 0.001	-	-	-
SCAFFOLD	NEIMS	0.582 ± 0.003	-	-	-

Table 2. Compound Retrieval (InChIKey Split): Top- k Accuracy for different values of k , best scores are in bold.

MODEL	TOP-1 \uparrow	TOP-3 \uparrow	TOP-5 \uparrow	TOP-10 \uparrow
FRAGNNET-D4	23.8%	50.4%	65.2%	83.1%
FRAGNNET-D3	23.3%	50.1%	63.8%	81.2%
ICEBERG	23.0%	48.5%	62.1%	78.9%
MASSFORMER	12.0%	30.4%	43.0%	62.9%
NEIMS	13.6%	32.3%	43.5%	62.7%

Table 3. Ensemble Annotation Consistency Comparison: CV is coefficient of variation, CONS is annotation consensus, MAJ is agreement with majority annotation.

METRIC	ENTROPY ENS	STANDARD ENS
MEAN COS_{HUN}	0.667	0.669
CV COS_{HUN}	0.116	0.115
MEAN $\hat{H}_\theta(n f)$	0.464	0.450
CV $\hat{H}_\theta(n f)$	0.512	0.216
CONS $\arg \max_n P_\theta(n f)$	0.745	0.818
MAJ $\arg \max_n P_\theta(n f)$	0.922	0.939

comparable average performance could be a useful strategy for flagging unreliable annotations.

To investigate annotation consistency, we trained two separate ensembles of 15 FraGNNNet-D3 models. The *Standard Ensemble* is composed of models without entropy regularization ($\alpha_{n|f} = 0$). The *Entropy Ensemble* is composed of five models with high entropy ($\alpha_{n|f} < 0$), five models with low entropy ($\alpha_{n|f} > 0$), and five models without regularization ($\alpha_{n|f} = 0$). Aside from entropy regularization, all models use the same optimization hyperparameters and only differ by initialization seed.

Table 3 demonstrates how these two ensembles achieve comparable average cosine similarity, but differ significantly in annotation distribution $P_\theta(n|f)$. The Entropy Ensemble experiences more variability in latent entropy $\hat{H}_\theta(n|f)$, with a coefficient of variation that is roughly twice as large as that of the Standard Ensemble. Trends in entropy are reflected in annotation agreement: the Entropy Ensemble has a lower average rate of annotation consensus than the Standard Ensemble (0.745 vs 0.818). Additionally, the average fraction of individual models that agree with the ensemble majority vote is lower in the Entropy Ensemble (0.922 vs 0.939). These trends are also reflected in the isomorphic annotation distribution $P_\theta(\tilde{n}|f)$ (Appendix J), although the entropy variations and resulting annotation disagreements are lower in comparison to those associated with $P_\theta(n|f)$.

Altogether, these results demonstrate how ensembles can be used to identify unreliable FraGNNNet structure annotations. Furthermore, they suggest that ensembling models with different latent entropies can improve sensitivity to annotation ambiguity without sacrificing performance.

6. Discussion

In this work we introduce FraGNNNet, a deep probabilistic model for spectrum prediction. Our work shows that pairing combinatorial fragmentation with neural networks can achieve state-of-the-art C2MS performance. FraGNNNet is unique in its interpretable latent representation of the fragmentation DAG. Features such as OS prediction and tunable entropy regularization further differentiate it from existing models. Strong results in the compound retrieval task demonstrate potential utility in MS2C applications.

Several aspects of our approach could be improved. The DAG calculation is a computational bottleneck, requiring recursive bond-removal operations. Additionally, the presence

of OS peaks are a reflection of an imperfect fragmentation model, which cannot be fixed with better optimization or more data. Complex reactions like cyclizations are difficult to model, since they introduce an explosion in the size of the fragment space. Developing a method that samples chemical reactions could be a viable solution for identifying fragments that cannot be generated by simple bond-breaking. Alternatively, ensembling FraGNNNet with a more flexible C2MS model, such as a binned predictor, could be an effective method of capturing OS peaks. Finally, adding support for unmerged spectrum prediction and increasing precursor adduct coverage are straightforward improvements that would broaden FraGNNNet’s practical applicability to MS2C tasks.

References

- Allen, F., Greiner, R., and Wishart, D. Competitive fragmentation modeling of ESI-MS/MS spectra for putative metabolite identification. *Metabolomics*, 11(1):98–110, February 2015. ISSN 1573-3890. doi: 10.1007/s11306-014-0676-4. URL <https://doi.org/10.1007/s11306-014-0676-4>.
- Battaglia, P. W., Hamrick, J. B., Bapst, V., Sanchez-Gonzalez, A., Zambaldi, V., Malinowski, M., Tacchetti, A., Raposo, D., Santoro, A., Faulkner, R., Gulcehre, C., Song, F., Ballard, A., Gilmer, J., Dahl, G., Vaswani, A., Allen, K., Nash, C., Langston, V., Dyer, C., Heess, N., Wierstra, D., Kohli, P., Botvinick, M., Vinyals, O., Li, Y., and Pascanu, R. Relational inductive biases, deep learning, and graph networks. *arXiv:1806.01261 [cs, stat]*, October 2018. URL <http://arxiv.org/abs/1806.01261>.
- Behnel, S., Bradshaw, R., Citro, C., Dalcin, L., Seljebotn, D. S., and Smith, K. Cython: The best of both worlds. *Computing in Science & Engineering*, 13(2):31–39, 2011.
- Bemis, G. W. and Murcko, M. A. The Properties of Known Drugs. 1. Molecular Frameworks. *Journal of Medicinal Chemistry*, 39(15):2887–2893, January 1996. ISSN 0022-2623. doi: 10.1021/jm9602928. URL <https://doi.org/10.1021/jm9602928>.
- Biemann, K. The application of mass spectrometry in organic chemistry: Determination of the structure of natural products. *Angewandte Chemie International Edition in English*, 1(2):98–111, 1962. doi: <https://doi.org/10.1002/anie.196200981>. URL <https://onlinelibrary.wiley.com/doi/abs/10.1002/anie.196200981>.
- Biewald, L. Experiment tracking with weights and biases, 2020. URL <https://www.wandb.com/>. Software available from wandb.com.
- Butler, T., Frandsen, A., Lighthouse, R., Bargh, B., Taylor, J., Bollerman, T. J., Kerby, T., West, K., Voronov, G., Moon, K., Kind, T., Dorrestein, P., Allen, A., Colluru, V., and Healey, D. MS2mol: A transformer model for illuminating dark chemical space from mass spectra, 2023. URL <https://chemrxiv.org/engage/chemrxiv/article-details/6492507524989702c2b082fc>.
- Dueñas, M. E., Peltier-Heap, R. E., Leveridge, M., Annan, R. S., Büttner, F. H., and Trost, M. Advances in high-throughput mass spectrometry in drug discovery. *EMBO Molecular Medicine*, 15(1):e14850, December 2022. ISSN 1757-4676. doi: 10.15252/emmm.202114850. URL <https://www.ncbi.nlm.nih.gov/pmc/articles/PMC9832828/>.
- Dührkop, K., Shen, H., Meusel, M., Rousu, J., and Böcker, S. Searching molecular structure databases with tandem mass spectra using csi:fingerid. *Proceedings of the National Academy of Sciences*, 112(41):12580–12585, 2015. ISSN 0027-8424. doi: 10.1073/pnas.1509788112. URL <https://www.pnas.org/content/112/41/12580>.
- Durant, J. L., Leland, B. A., Henry, D. R., and Nourse, J. G. Reoptimization of MDL keys for use in drug discovery. *Journal of Chemical Information and Computer Sciences*, 42(6):1273–1280, 2002. ISSN 0095-2338. doi: 10.1021/ci010132r.
- Dührkop, K., Fleischauer, M., Ludwig, M., Aksenov, A. A., Melnik, A. V., Meusel, M., Dorrestein, P. C., Rousu, J., and Böcker, S. SIRIUS 4: a rapid tool for turning tandem mass spectra into metabolite structure information. *Nature Methods*, 16(4):299–302, April 2019. ISSN 1548-7105. doi: 10.1038/s41592-019-0344-8. URL <http://www.nature.com/articles/s41592-019-0344-8>.
- Falcon, W. and The PyTorch Lightning team. PyTorch Lightning, March 2019. URL <https://github.com/Lightning-AI/lightning>.
- Fey, M. and Lenssen, J. E. Fast graph representation learning with pytorch geometric. *CoRR*, abs/1903.02428, 2019. URL <http://arxiv.org/abs/1903.02428>.
- Goldman, S., Bradshaw, J., Xin, J., and Coley, C. Prefix-Tree Decoding for Predicting Mass Spectra from Molecules. In Oh, A., Neumann, T., Globerson, A., Saenko, K., Hardt, M., and Levine, S. (eds.), *Advances in Neural Information Processing Systems*, volume 36, pp. 48548–48572. Curran Associates, Inc., 2023a. URL https://proceedings.neurips.cc/paper_files/paper/2023/file/97d596ca21d07

- 51ba2c633bad696cf7f-Paper-Conference.pdf.
- Goldman, S., Wohlwend, J., Stražar, M., Haroush, G., Xavier, R. J., and Coley, C. W. Annotating metabolite mass spectra with domain-inspired chemical formula transformers. *Nature Machine Intelligence*, 5(9):965–979, 2023b. ISSN 2522-5839. doi: 10.1038/s42256-023-0708-3. URL <https://www.nature.com/articles/s42256-023-00708-3>. Number: 9 Publisher: Nature Publishing Group.
- Goldman, S., Xin, J., Provenzano, J., and Coley, C. W. MIST-CF: Chemical Formula Inference from Tandem Mass Spectra. *Journal of Chemical Information and Modeling*, September 2023c. ISSN 1549-9596. doi: 10.1021/acs.jcim.3c01082. URL <https://doi.org/10.1021/acs.jcim.3c01082>. Publisher: American Chemical Society.
- Goldman, S., Li, J., and Coley, C. W. Generating Molecular Fragmentation Graphs with Autoregressive Neural Networks. *Analytical Chemistry*, 96(8):3419–3428, February 2024. ISSN 0003-2700. doi: 10.1021/acs.analchem.3c04654. URL <https://doi.org/10.1021/acs.analchem.3c04654>. Publisher: American Chemical Society.
- Gowda, G. N. and Djukovic, D. Overview of Mass Spectrometry-Based Metabolomics: Opportunities and Challenges. *Methods in molecular biology (Clifton, N.J.)*, 1198:3–12, 2014. ISSN 1064-3745. doi: 10.1007/978-1-4939-1258-2_1. URL <https://www.ncbi.nlm.nih.gov/pmc/articles/PMC4336784/>.
- Hagberg, A., Swart, P., and S Chult, D. Exploring network structure, dynamics, and function using networkx. Technical report, Los Alamos National Lab.(LANL), Los Alamos, NM (United States), 2008.
- Heller, S. R., McNaught, A., Pletnev, I., Stein, S., and Tchekhovskoi, D. InChI, the IUPAC International Chemical Identifier. *Journal of Cheminformatics*, 7(1):23, May 2015. ISSN 1758-2946. doi: 10.1186/s13321-015-0068-4. URL <https://doi.org/10.1186/s13321-015-0068-4>.
- Hong, Y., Li, S., Welch, C. J., Tichy, S., Ye, Y., and Tang, H. 3DMolMS: prediction of tandem mass spectra from 3D molecular conformations. *Bioinformatics*, 39(6):btad354, May 2023. ISSN 1367-4811. doi: 10.1093/bioinformatics/btad354. URL <https://doi.org/10.1093/bioinformatics/btad354>. eprint: <https://academic.oup.com/bioinformatics/article-pdf/39/6/btad354/50661428/btad354.pdf>.
- Huber, F., Verhoeven, S., Meijer, C., Spreeuw, H., Castilla, E. M. V., Geng, C., Hooft, J. J. j. v. d., Rogers, S., Belloum, A., Diblen, F., and Spaaks, J. H. matchms - processing and similarity evaluation of mass spectrometry data. *Journal of Open Source Software*, 5(52):2411, August 2020. ISSN 2475-9066. doi: 10.21105/joss.02411. URL <https://joss.theoj.org/papers/10.21105/joss.02411>.
- Kim, S., Chen, J., Cheng, T., Gindulyte, A., He, J., He, S., Li, Q., Shoemaker, B. A., Thiessen, P. A., Yu, B., Zaslavsky, L., Zhang, J., and Bolton, E. E. PubChem 2019 update: improved access to chemical data. *Nucleic Acids Research*, 47(Database issue):D1102–D1109, January 2019. ISSN 0305-1048. doi: 10.1093/nar/gky1033. URL <https://www.ncbi.nlm.nih.gov/pmc/articles/PMC6324075/>.
- Kong, K., Li, G., Ding, M., Wu, Z., Zhu, C., Ghanem, B., Taylor, G., and Goldstein, T. Robust optimization as data augmentation for large-scale graphs. In *Proceedings of the IEEE/CVF Conference on Computer Vision and Pattern Recognition*, pp. 60–69, 2022.
- Kuhn, H. W. The Hungarian method for the assignment problem. *Naval Research Logistics Quarterly*, 2(1-2): 83–97, March 1955. ISSN 0028-1441, 1931-9193. doi: 10.1002/nav.3800020109. URL <https://onlinelibrary.wiley.com/doi/10.1002/nav.3800020109>.
- Lakshminarayanan, B., Pritzel, A., and Blundell, C. Simple and Scalable Predictive Uncertainty Estimation using Deep Ensembles. In *Advances in Neural Information Processing Systems*, volume 30. Curran Associates, Inc., 2017. URL https://proceedings.neurips.cc/paper_files/paper/2017/hash/9ef2ed4b7fd2c810847ffa5fa85bce38-Abstract.html.
- Landrum, G. Rdkit: Open-source cheminformatics, 2022. URL <http://www.rdkit.org>.
- Lebedev, A. T. Environmental Mass Spectrometry. *Annual Review of Analytical Chemistry*, 6(1):163–189, 2013. doi: 10.1146/annurev-anchem-062012-092604. URL <https://doi.org/10.1146/annurev-anchem-062012-092604>.
- Li, X., Zhu, H., Liu, L.-p., and Hassoun, S. Ensemble Spectral Prediction (ESP) Model for Metabolite Annotation. *arXiv:2203.13783 [cs, q-bio]*, March 2022. URL <http://arxiv.org/abs/2203.13783>. arXiv: 2203.13783.
- McLafferty, F. W. Mass Spectrometric Analysis. Molecular Rearrangements. *Analytical Chemistry*, 31(1):82–87, January 1959. ISSN 0003-2700. doi: 10.1021/ac60145a015.

- URL <https://doi.org/10.1021/ac60145a015>. Publisher: American Chemical Society.
- Murphy, M., Jegelka, S., Fraenkel, E., Kind, T., Healey, D., and Butler, T. Efficiently predicting high resolution mass spectra with graph neural networks. In Krause, A., Brunskill, E., Cho, K., Engelhardt, B., Sabato, S., and Scarlett, J. (eds.), *Proceedings of the 40th International Conference on Machine Learning*, volume 202 of *Proceedings of Machine Learning Research*, pp. 25549–25562. PMLR, July 2023. URL <https://proceedings.mlr.press/v202/murphy23a.html>.
- Nakata, M. and Shimazaki, T. PubChemQC Project: A Large-Scale First-Principles Electronic Structure Database for Data-Driven Chemistry. *Journal of Chemical Information and Modeling*, 57(6):1300–1308, June 2017. ISSN 1549-9596. doi: 10.1021/acs.jcim.7b00083. URL <https://doi.org/10.1021/acs.jcim.7b00083>.
- Paszke, A., Gross, S., Massa, F., Lerer, A., Bradbury, J., Chanan, G., Killeen, T., Lin, Z., Gimelshein, N., Antiga, L., Desmaison, A., Köpf, A., Yang, E., DeVito, Z., Raison, M., Tejani, A., Chilamkurthy, S., Steiner, B., Fang, L., Bai, J., and Chintala, S. PyTorch: An Imperative Style, High-Performance Deep Learning Library. *arXiv:1912.01703 [cs, stat]*, December 2019. URL <http://arxiv.org/abs/1912.01703>.
- Peters, F. T. Recent advances of liquid chromatography–(tandem) mass spectrometry in clinical and forensic toxicology. *Clinical Biochemistry*, 44(1):54–65, January 2011. ISSN 0009-9120. doi: 10.1016/j.clinbiochem.2010.08.008. URL <https://www.sciencedirect.com/science/article/pii/S000991201003486>.
- Python Core Team. *Python: A dynamic, open source programming language*. Python Software Foundation, 2021. URL <https://www.python.org/>.
- Ridder, L., Hooft, J. J. J. v. d., and Verhoeven, S. Automatic Compound Annotation from Mass Spectrometry Data Using MAGMa. *Mass Spectrometry*, 3(Special_Issue_2):S0033–S0033, 2014. doi: 10.5702/massspectrometry.S0033.
- Rogers, D. and Hahn, M. Extended-Connectivity Fingerprints. *Journal of Chemical Information and Modeling*, 50(5):742–754, May 2010. ISSN 1549-9596. doi: 10.1021/ci100050t. URL <https://doi.org/10.1021/ci100050t>.
- Ruttkies, C., Schymanski, E. L., Wolf, S., Hollender, J., and Neumann, S. MetFrag relaunched: incorporating strategies beyond in silico fragmentation. *Journal of Cheminformatics*, 8(1):3, January 2016. ISSN 1758-2946. doi: 10.1186/s13321-016-0115-9. URL <https://doi.org/10.1186/s13321-016-0115-9>.
- Schymanski, E. L., Ruttkies, C., Krauss, M., Brouard, C., Kind, T., Dührkop, K., Allen, F., Vaniya, A., Verdegem, D., Böcker, S., Rousu, J., Shen, H., Tsugawa, H., Sajed, T., Fiehn, O., Ghesquière, B., and Neumann, S. Critical Assessment of Small Molecule Identification 2016: automated methods. *Journal of Cheminformatics*, 9(1):22, March 2017. ISSN 1758-2946. doi: 10.1186/s13321-017-0207-1. URL <https://doi.org/10.1186/s13321-017-0207-1>.
- Shervashidze, N., Schweitzer, P., Leeuwen, E. J. v., Mehlhorn, K., and Borgwardt, K. M. Weisfeiler-Lehman Graph Kernels. *Journal of Machine Learning Research*, 12(77):2539–2561, 2011. URL <http://jmlr.org/papers/v12/shervashidzella.html>.
- Shrivastava, A. D., Swainston, N., Samanta, S., Roberts, I., Wright Muelas, M., and Kell, D. B. MassGenie: A Transformer-Based Deep Learning Method for Identifying Small Molecules from Their Mass Spectra. *Biomolecules*, 11(12):1793, November 2021. ISSN 2218-273X. doi: 10.3390/biom11121793. URL <https://www.ncbi.nlm.nih.gov/pmc/articles/PMC8699281/>.
- Skinninger, M. A., Wang, F., Pasin, D., Greiner, R., Foster, L. J., Dalsgaard, P. W., and Wishart, D. S. A deep generative model enables automated structure elucidation of novel psychoactive substances. *Nature Machine Intelligence*, 3(11):973–984, November 2021. ISSN 2522-5839. doi: 10.1038/s42256-021-00407-x. URL <https://www.nature.com/articles/s42256-021-00407-x>. Number: 11 Publisher: Nature Publishing Group.
- Stein, S. Mass Spectral Reference Libraries: An Ever-Expanding Resource for Chemical Identification. *Analytical Chemistry*, 84(17):7274–7282, September 2012. ISSN 0003-2700. doi: 10.1021/ac301205z. URL <https://doi.org/10.1021/ac301205z>.
- Stein, S. E. and Scott, D. R. Optimization and testing of mass spectral library search algorithms for compound identification. *Journal of the American Society for Mass Spectrometry*, 5(9):859–866, September 1994. ISSN 1044-0305. doi: 10.1016/1044-0305(94)87009-8. URL <https://pubs.acs.org/doi/10.1016/1044-0305%2894%2987009-8>.
- Stravs, M. A., Dührkop, K., Böcker, S., and Zamboni, N. MSNovelist: de novo structure generation from mass spectra. *Nature Methods*, 19(7):865–870, July 2022. ISSN 1548-7105. doi: 10.1038/s41592-022-01486-3.

- URL <https://www.nature.com/articles/s41592-022-01486-3>. Number: 7 Publisher: Nature Publishing Group.
- Tancik, M., Srinivasan, P. P., Mildenhall, B., Fridovich-Keil, S., Raghavan, N., Singhal, U., Ramamoorthi, R., Barron, J. T., and Ng, R. Fourier features let networks learn high frequency functions in low dimensional domains. *CoRR*, abs/2006.10739, 2020. URL <https://arxiv.org/abs/2006.10739>.
- van Tetering, L., Spies, S., Wildeman, Q. D. K., Houthuijs, K. J., van Outersterp, R. E., Martens, J., Wevers, R. A., Wishart, D. S., Berden, G., and Oomens, J. A spectroscopic test suggests that fragment ion structure annotations in MS/MS libraries are frequently incorrect. *Communications Chemistry*, 7(1):1–11, February 2024. ISSN 2399-3669. doi: 10.1038/s42004-024-01112-7. URL <https://www.nature.com/articles/s42004-024-01112-7>. Number: 1 Publisher: Nature Publishing Group.
- Voronov, G., Frandsen, A., Bargh, B., Healey, D., Lightheart, R., Kind, T., Dorrestein, P., Colluru, V., and Butler, T. Ms2prop: A machine learning model that directly predicts chemical properties from mass spectrometry data for novel compounds. *bioRxiv*, 2022. doi: 10.1101/2022.10.09.511482. URL <https://www.biorxiv.org/content/early/2022/10/11/2022.10.09.511482>.
- Wang, F., Liigand, J., Tian, S., Arndt, D., Greiner, R., and Wishart, D. S. CFM-ID 4.0: More Accurate ESI-MS/MS Spectral Prediction and Compound Identification. *Analytical Chemistry*, August 2021. ISSN 0003-2700. doi: 10.1021/acs.analchem.1c01465. URL <https://doi.org/10.1021/acs.analchem.1c01465>.
- Wang, F., Pasin, D., Skinnider, M. A., Liigand, J., Kleis, J.-N., Brown, D., Oler, E., Sajed, T., Gautam, V., Harrison, S., Greiner, R., Foster, L. J., Dalsgaard, P. W., and Wishart, D. S. Deep Learning-Enabled MS/MS Spectrum Prediction Facilitates Automated Identification Of Novel Psychoactive Substances. *Analytical Chemistry*, 95(50):18326–18334, December 2023. ISSN 0003-2700. doi: 10.1021/acs.analchem.3c02413. URL <https://doi.org/10.1021/acs.analchem.3c02413>. Publisher: American Chemical Society.
- Wei, J. N., Belanger, D., Adams, R. P., and Sculley, D. Rapid prediction of electron-ionization mass spectrometry using neural networks. *ACS Central Science*, 5(4): 700–708, April 2019. ISSN 2374-7943, 2374-7951. doi: 10.1021/acscentsci.9b00085. URL <https://pubs.acs.org/doi/10.1021/acscentsci.9b00085>.
- Wishart, D. S., Feunang, Y. D., Marcu, A., Guo, A. C., Liang, K., Vázquez-Fresno, R., Sajed, T., Johnson, D., Li, C., Karu, N., Sayeeda, Z., Lo, E., Assempour, N., Berjanskii, M., Singhal, S., Arndt, D., Liang, Y., Badran, H., Grant, J., Serra-Cayuela, A., Liu, Y., Mandal, R., Neveu, V., Pon, A., Knox, C., Wilson, M., Manach, C., and Scalbert, A. HMDB 4.0: the human metabolome database for 2018. *Nucleic Acids Research*, 46(D1):D608–D617, January 2018. ISSN 1362-4962. doi: 10.1093/nar/gkx1089.
- Wolf, S., Schmidt, S., Müller-Hannemann, M., and Neumann, S. In silico fragmentation for computer assisted identification of metabolite mass spectra. *BMC Bioinformatics*, 11(1):148, March 2010. ISSN 1471-2105. doi: 10.1186/1471-2105-11-148. URL <https://doi.org/10.1186/1471-2105-11-148>.
- Wu, Z., Ramsundar, B., Feinberg, E. N., Gomes, J., Geniesse, C., Pappu, A. S., Leswing, K., and Pande, V. MoleculeNet: a benchmark for molecular machine learning. *Chemical Science*, 9(2):513–530, January 2018. ISSN 2041-6539. doi: 10.1039/C7SC02664A. URL <https://pubs.rsc.org/en/content/articlelanding/2018/sc/c7sc02664a>. Publisher: The Royal Society of Chemistry.
- Xu, K., Hu, W., Leskovec, J., and Jegelka, S. How Powerful are Graph Neural Networks? September 2018. URL <https://openreview.net/forum?id=ryGs6iA5Km>.
- Yang, X., Neta, P., and Stein, S. E. Quality Control for Building Libraries from Electrospray Ionization Tandem Mass Spectra. *Analytical Chemistry*, 86(13):6393–6400, July 2014. ISSN 0003-2700, 1520-6882. doi: 10.1021/ac500711m. URL <https://pubs.acs.org/doi/10.1021/ac500711m>.
- Ying, C., Cai, T., Luo, S., Zheng, S., Ke, G., He, D., Shen, Y., and Liu, T.-Y. Do transformers really perform bad for graph representation? *Neural Information Processing Systems (NeurIPS)*, 2021.
- Young, A., Wang, B., and Röst, H. MassFormer: Tandem Mass Spectrum Prediction for Small Molecules using Graph Transformers, May 2023. URL <http://arxiv.org/abs/2111.04824>. arXiv:2111.04824 [cs, q-bio].
- Zhu, H., Liu, L., and Hassoun, S. Using Graph Neural Networks for Mass Spectrometry Prediction. *arXiv:2010.04661 [cs]*, October 2020. URL <http://arxiv.org/abs/2010.04661>.
- Zhu, R. L. and Jonas, E. Rapid Approximate Subset-Based Spectra Prediction for Electron Ionization–Mass Spec-

trometry. *Analytical Chemistry*, 95(5):2653–2663, February 2023. ISSN 0003-2700. doi: 10.1021/acs.analchem.2c02093. URL <https://doi.org/10.1021/acs.analchem.2c02093>. Publisher: American Chemical Society.

A. Recursive Fragmentation Algorithm

Algorithm 1 RecFrag

Input: heavy-atom subgraph $G = (V, E)$, max depth d , current depth d'

Initialize DAG nodes $V_F = \{\}$, DAG edges $E_F = \{\}$

if $d' \leq d$ **then**

$I = \text{ID}(V)$

for $e = (u, v) \in E$ **do**

$E' = E - \{e\}$

$(V^u, E^u) = \text{BFSCC}(u, V, E')$

$I^u = \text{ID}(V^u)$

$(V^v, E^v) = \text{BFSCC}(v, V, E')$

$I^v = \text{ID}(V^v)$

$S = S \cup \{(V^u, E^u), (V^v, E^v)\}$

$V_F = V_F \cup \{I^u, I^v\}$

$E_F = E_F \cup \{(I, I^u), (I, I^v)\}$

end for

for $G^s = (V^s, E^s) \in S$ **do**

$(V_F^s, E_F^s) = \text{RecFrag}(G^s, d, d' + 1)$

$V_F = V_F \cup V_F^s$

$E_F = E_F \cup E_F^s$

end for

end if

Return (V_F, E_F)

The approximate fragmentation DAG $G_{\mathcal{F}^d}$ is constructed by calling Algorithm 1 on the heavy-atom skeleton of the molecule $\mathcal{H}(G)$, with initial depth parameter $d' = 1$. BFSCC is a breadth-first search algorithm that returns the set of nodes and edges in a graph that can be reached from a given input node. ID is a function that takes a subset of the (ordered) graph nodes and maps them to a unique integer id (our implementation simply converts the binary representation of the subgraph node mask to a decimal integer).

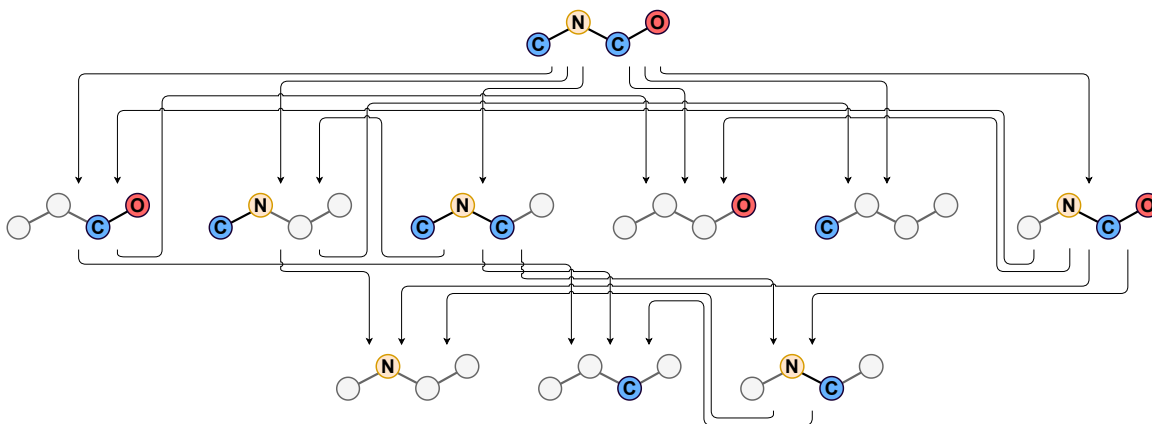


Figure 4. DAG Visualization: the approximate fragmentation DAG $G_{\mathcal{F}^d}$ ($d = 3$) for a small molecule, methylaminomethanol. The root node is represented by the heavy-atom skeleton of the molecule $\mathcal{H}(G)$, and each other node is represented by a subgraph of $\mathcal{H}(G)$. Carbon atoms are represented by “C”, nitrogen atoms by “N”, oxygen atoms by “O”.

Figure 4 is a visualization of the full fragmentation DAG \mathcal{F}_G for an example molecule. Since this molecule is small and linear, the resulting DAG consists of only 10 nodes and 19 edges.

B. Fragmentation DAG Statistics

Table 4. Fragmentation DAG Statistics over the NIST20 Dataset (first and third quartiles).

STATISTIC	$d = 3, j = 4$	$d = 4, j = 4$
# FORMULAE f	325 – 849	390 – 1179
# NODES n	167 – 482	334 – 1425
# NODES \tilde{n}	104 – 313	184 – 886
# EDGES e	662 – 2170	2296 – 10251
RECALL (0.01 DA)	0.600 – 0.821	0.727 – 0.898
RECALL (10 PPM)	0.485 – 0.733	0.597 – 0.817
WEIGHTED RECALL (0.01 DA)	0.773 – 0.967	0.885 – 0.985
WEIGHTED RECALL (10 PPM)	0.730 – 0.952	0.846 – 0.973

Table 4 describes the size of approximate fragmentation DAG $G_{\mathcal{F}^d}$ and the coverage of its associated mass set $\hat{M}(G, d, j)$ under two different parameterizations. $d = 3, j = 4$ is the configuration used by FraGNNNet-D3, and $d = 4, j = 4$ is the configuration for FraGNNNet-D4.

Recall (R) is measured as the fraction of peaks in the spectrum that can be explained by a mass (Equation 10) while weighted recall (WR) incorporates peak intensities (Equation 11).

$$R(G_{\mathcal{F}^d}, P(m)) = \sum_{m \in M} \mathbb{I}[\exists n \in V_{\mathcal{F}^d} : \|m_n - m\| \leq \tau_{m_n, m}] \quad (10)$$

$$WR(G_{\mathcal{F}^d}, P(m)) = \sum_{m \in M} P(m) \mathbb{I}[\exists n \in V_{\mathcal{F}^d} : \|m_n - m\| \leq \tau_{m_n, m}] \quad (11)$$

For the 0.01 Da approach $\tau_{m_n, m} = 0.01$, while for the 10 ppm approach $\tau_{m_n, m} = 10^{-5} \max(m_n, m)$. In our experiments, the output distribution $P_\theta(m)$ is defined such that $P_\theta(m) = 0$ iff $\nexists n \in V_{\mathcal{F}^d} : \|m_n - m\| \leq 10^{-5} \max(m_n, m)$. Under this definition of the output distribution, weighted recall with 10ppm tolerance is equivalent to the probability $P(M^{IS}) = 1 - P(M^{OS})$.

C. Conceptual Comparisons with Related C2MS Models

In this section, we contrast FraGNNNet with two other closely-related structured C2MS models: CFM and ICEBERG.

CFM (Competitive Fragmentation Modelling, Allen et al. 2015; Wang et al. 2021) is the most widely used C2MS tool. Like FraGNNNet, it uses a combinatorially generated fragmentation DAG to model a distribution over fragments. However, the level of detail in the DAG is much greater. CFM explicitly models the location of hydrogens and higher order bonds, and implements several complex fragmentation reactions (McLafferty, 1959; Biemann, 1962) that our method does not. In principle, CFM can produce higher quality peak annotations than FraGNNNet, since each fragment is (likely) a valid chemical chemical structure and not simply a heavy-atom subgraph and associated hydrogen count. However, this interpretability comes at a cost: the DAG construction step can last over an hour for very large molecules due to its complexity. We do not directly compare with CFM due to difficulties in scaling the model training to larger datasets such as NIST20 (Goldman et al., 2023a; 2024; Murphy et al., 2023). Furthermore, previous work from the literature has demonstrated that it is outperformed by more recent C2MS models (Young et al., 2023; Murphy et al., 2023; Goldman et al., 2024).

ICEBERG (Inferring Collision-induced-dissociation by Estimating Breakage Events and Reconstructing their Graphs, Goldman et al. 2024) is a state-of-the-art C2MS model. As outlined in Section 5.1, ICEBERG is composed of two sub-modules. The first module (the *fragment generator*) autoregressively predicts a simplified fragmentation DAG, and the second module (the *intensity predictor*) outputs a distribution over those fragments. The fragment generator is trained to approximate a fragmentation tree that is constructed by a variant of the MAGMa algorithm (Ridder et al., 2014). MAGMa applies a combinatorial atom removal strategy to generate a fragmentation DAG from an input molecular graph G : the resulting DAG has a similar set of fragment nodes to $G_{\mathcal{F}^d}$, but may contain different edges (refer to Ridder et al. 2014; Goldman et al. 2024 for full details). The MAGMa DAG is then simplified using a number of pruning strategies. Fragments

with masses that are not represented by any peak in the spectrum are removed, as are fragments that map to same peak as another (chemical heuristics are used to determine which fragment should be kept in such cases). Unlike our approach, no distinction is made between isomorphic fragments that originate from different parts of the molecule. Redundant paths between fragments are removed to convert the DAG into a proper tree, which is required for autoregressive generation.

ICEBERG’s aggressive pruning removes information from the DAG that could be important for correctly predicting the spectrum. However, this pruning also facilitates more expressive representations of the fragments that remain: since the total number of fragments is lower, the computational and memory cost per fragment can be much higher. This tradeoff underlines the key conceptual difference between FraGNNNet and ICEBERG. The former uses a more complete fragmentation DAG but must employ a simpler representation for each individual fragment. The latter can afford a more complex fragment representation but only considers a small subset of the DAG. Our experiments in Section 5.1 suggest that retaining DAG information may be important, since FraGNNNet outperforms both ICEBERG (which uses a stochastic approximation to the pruned DAG) and ICEBERG-ADV (which uses extra information from the spectrum to exactly calculate the pruned DAG).

Note that DAG node pruning might also affect predicted peak annotations. Our experiments in Section 5.3 suggest that it is plausible for a single peak to map to multiple fragments, as indicated by non-zero annotation entropies $H_\theta(n|f)$. Compared to FraGNNNet, ICEBERG is much more restricted in its ability to model such fragments, preventing it from considering the entire set of plausible annotations.

D. Fragment Subgraph Isomorphism

In mass spectrometry, it is possible for fragments with identical molecular structure to originate from different parts of the molecular graph, having been created through distinct sequences of fragmentation steps. In our model, this phenomenon is represented by pairs of DAG nodes $n_1, n_2 \in V_{\mathcal{F}^d}$ whose corresponding subgraphs $G_{n_1} \cong G_{n_2}$ are isomorphic (i.e. there exists a node bijection between G_{n_1} and G_{n_2} that is both label-preserving and edge-preserving).

With the exception of $P_\theta(f)$ (which does not involve fragments), each of the latent distributions from Section 4.3 can be adapted to account for fragment graph isomorphism. To describe this process precisely, we rely on Definition D.1 and Corollary D.2:

Definition D.1. Let \mathcal{G} be a finite set of labelled graphs $\{G_i\}_{i=1}^I$. Each G_i is a member of one of K isomorphism classes $\{\mathcal{G}_k\}_{k=1}^K$, $K \leq I$. Assume an arbitrary total ordering \prec_k for each isomorphic class \mathcal{G}_k . Let $\mathcal{I}(\mathcal{G}) \subseteq \mathcal{G}$ be the set of graphs such that $\forall G_k \in \mathcal{I}(\mathcal{G}) : \nexists G_i \in \mathcal{G} : G_i \in \mathcal{G}_k \wedge G_i \prec_k G_k$.

Corollary D.2. $\forall G_1, G_2 \in \mathcal{I}(\mathcal{G}) : G_1 \neq G_2 \rightarrow G_1 \not\cong G_2$.

For each DAG node \tilde{n} such that $G_{\tilde{n}} \in \mathcal{I}(\{G_n : n \in V_{\mathcal{F}^d}\})$, we define $P_\theta(\tilde{n})$ as the total probability of all subgraphs isomorphic to $G_{\tilde{n}}$ using Equation 12:

$$P_\theta(\tilde{n}) = \sum_{n \in V_{\mathcal{F}^d} : G_n \cong G_{\tilde{n}}} P_\theta(n) \quad (12)$$

The conditional distributions $P_\theta(f|\tilde{n})$ and $P_\theta(\tilde{n}|f)$ are defined in a similar manner using Equations 13 and 14 respectively:

$$P_\theta(f|\tilde{n}) = \sum_{n \in V_{\mathcal{F}^d} : G_n \cong G_{\tilde{n}}} \frac{P_\theta(f|n)P_\theta(n)}{P_\theta(\tilde{n})} \quad (13)$$

$$P_\theta(\tilde{n}|f) = \sum_{n \in V_{\mathcal{F}^d} : G_n \cong G_{\tilde{n}}} P_\theta(n|f) \quad (14)$$

These distributions can provide additional insight into model behaviour, as demonstrated in Appendix J. Intuitively, they remove excess entropy caused by uncertainty over the location in the molecule from which a particular fragment originated.

In practice, we calculate the set $\mathcal{I}(\{G_n : n \in V_{\mathcal{F}^d}\})$ by applying an approximate Weisfeiler-Lehman hashing algorithm (Shervashidze et al., 2011; Hagberg et al., 2008) to each subgraph $G_n : n \in V_{\mathcal{F}^d}$ and identify isomorphism class membership using the resulting hashes.

E. Molecule Features

Table 5. Input Features for the Molecule GNN

FEATURE	VALUES
ATOM TYPE (ELEMENT)	{C, O, N, P, S, F, Cl, Br, I, Se, Si}
ATOM DEGREE	{0, ..., 10}
ATOM ORBITAL HYBRIDIZATION	{SP, SP2, SP3, SP3D, SP3D2}
ATOM FORMAL CHARGE	{-2, ..., +2}
ATOM RADICAL STATE	{0, ..., 4}
ATOM RING MEMBERSHIP	{TRUE, FALSE}
ATOM AROMATIC	{TRUE, FALSE}
ATOM MASS	\mathbb{R}^+
ATOM CHIRALITY	{UNSPECIFIED, TETRAHEDRAL CW, TETRAHEDRAL CCW}
BOND DEGREE	{SINGLE, DOUBLE, TRIPLE, AROMATIC}

Our method for atom and bond featurization follows the approach taken by (Goldman et al., 2024). The features are summarized in Table 5. All discrete features are encoded using a standard one-hot representation. The only continuous feature (Atom Mass) is scaled by a factor of 0.01.

F. Fragment Features

F.1. Fourier Embeddings

We use Fourier embeddings (Goldman et al., 2023a; Tancik et al., 2020) to represent certain ordinal features such as mass formulae and collision energies. Given an integer feature $z \in \mathbb{R}$, the corresponding Fourier embedding $\phi(z)$ can be calculated using Equation 15:

$$\phi(z) = \left[\left| \sin \left(\frac{2\pi z}{\tau_1} \right) \right|, \dots, \left| \sin \left(\frac{2\pi z}{\tau_T} \right) \right| \right] \quad (15)$$

In principle, it may be easier for the model to handle inputs z at inference that have not been seen in training when compared with a standard one-hot encoding scheme. The periods τ_t are increasing powers of 2 (we use $T = 10$ for our experiments).

F.2. DAG Node Features

The DAG node embeddings (Equation 4) are initialized with formula information \hat{h}_n^f and fragmentation depth information \hat{h}_n^d . The formula embedding for DAG node n is a concatenation of Fourier embeddings corresponding to heavy atom counts in G_n , described in Equation 16:

$$\hat{h}_n^f = \left\| \left\| \phi \left(\sum_{v \in V_n} \omega_v = \omega \right) \right. \right. \quad (16)$$

The depth embedding \hat{h}_n^d is a multi-hot representation of the fragment node’s depth in the DAG. The depth set is defined as the set of path lengths between the root node and the fragment node n , and is always a subset of $\{0, \dots, d\}$ where d is the fragmentation depth.

F.3. DAG Edge Features

The embeddings $\bar{h}_e^{(0)}$ are initialized for each directed edge $e \in E_{\mathcal{F}^d}$ using Equation 17. Assuming e travels from node n to node t , let $V_e = V_n - V_t$ be the set of atoms in G_n that are not in G_t . As described in Equation 18, \hat{h}_e^s is simply the average of the atom embeddings in V_e .

$$\bar{h}_e^{(0)} = \hat{h}_e^s \parallel \hat{h}_e^f \quad (17)$$

$$\hat{h}_e^s = \frac{1}{|V_e|} \sum_{a \in V_e} \bar{h}_a^{(L_1)} \quad (18)$$

The \hat{h}_e^f term is an embedding of the difference of node formulas $f_n - f_t$ using Fourier embeddings, similar to \hat{h}_e^f . These features explicitly capture neutral loss information that would otherwise need to be inferred from the DAG.

F.4. Collision Energy Embedding

Let Z_i be the set of collision energies that were merged to create spectrum Y_i for molecule X_i in the dataset. The collision energy embedding is a representation of Z_i . Each collision energy $z \in Z_i$ is a positive integer ranging from 0 to 200 (they are normalized relative to the mass of the precursor, see Young et al. 2023 for more details). The collision energy embedding \hat{h}_Z is simply an average of Fourier embeddings for each collision energy, described by Equation 19:

$$\hat{h}_Z = \frac{1}{|Z|} \sum_{z \in Z} f(z) \quad (19)$$

The collision energy embedding \hat{h}_Z is concatenated with the output Fragment GNN embedding $\bar{h}_n^{(L_2)}$ for each DAG node $n \in G_{\mathcal{F}d}$ before being passed to the output MLP.

G. Spectrum Similarity Metrics

Mass spectra are typically compared using a form of cosine similarity (Stein & Scott, 1994). The binned approach involves discretizing each spectrum into a 1-dimensional vector of intensities, and calculating the cosine similarity between the spectrum vectors (Wei et al., 2019; Young et al., 2023; Zhu et al., 2020). In our experiments, binned cosine similarity $COS_{0.01}$ is calculated with a bin size of 0.01 Da. An alternate approach measures similarity by matching peaks that are close in mass (Huber et al., 2020; Murphy et al., 2023). This can be formalized as the linear sum assignment problem below, where i indexes spectrum Y , j indexes spectrum \hat{Y} and p_i, \hat{p}_j are shorthand for $P(m_i), \hat{P}(\hat{m}_j)$ respectively:

$$\begin{aligned} COS_{\text{HUN}}(Y, \hat{Y}) &= \max_{w_{ij} \in \{0,1\}} \sum_{i,j} w_{ij} \frac{p_i}{\|p\|_2} \frac{\hat{p}_j}{\|\hat{p}\|_2} \\ \text{s.t.} &\begin{cases} \sum_i w_{ij} \leq 1 \\ \sum_j w_{ij} \leq 1 \\ |m_i - \hat{m}_j| \leq \tau_{ij} \end{cases} \end{aligned} \quad (20)$$

We set the tolerance parameter $\tau_{ij} = 10^{-5} \max(m_i, \hat{m}_j)$ to reflect a 10ppm mass error. This maximization problem can be solved efficiently using the Hungarian algorithm (Kuhn, 1955).

H. Model Ablations

We perform two kinds of ablations: (-CE) corresponds to the removal of merged collision energy information (Appendix F.4), (+Edges) corresponds to the addition of edge embeddings and message passing in the Fragment GNN. The removal of collision energy information seems to have a significant impact on both FraGNNNet-D3 and FraGNNNet-D4 performance, while the addition of DAG edge information does not seem to have a strong effect.

Table 6. Model Ablations: Performance reported on validation set, mean and standard of 5 random seeds. Best scores are in bold

MODEL	$COS_{0.01} \uparrow$	$COS_{HUN} \uparrow$
FRAGNNET-D3	.693 ± .003	.668 ± .001
FRAGNNET-D3 (-CE)	.681 ± .002	.656 ± .001
FRAGNNET-D3 (+EDGES)	.693 ± .003	.667 ± .001
FRAGNNET-D4	.709 ± .001	.684 ± .001
FRAGNNET-D4 (-CE)	.693 ± .001	.670 ± .001
FRAGNNET-D4 (+EDGES)	.711 ± .002	.687 ± .001

I. Datasets and Splits

We train and evaluate all models on the NIST 2020 MS/MS dataset (Stein, 2012; Yang et al., 2014), a large commercial library of MS data. To ensure homogeneity, the original dataset is filtered for $[M+H]^+$ spectra from Orbitrap instruments. Following (Young et al., 2023; Goldman et al., 2024), spectra for the same compound acquired at different collision energies are averaged (a process commonly referred to as *collision energy merging*). The resulting dataset contains 21,114 unique molecules and their merged spectra. Models are trained using 60% of the data, with 20% for validation and 20% used as a heldout test set. Two strategies for data splitting are employed: a simple random split by molecule ID using the InChIKey hashing algorithm (Heller et al., 2015), and a more challenging split that clusters molecules based on their Murcko Scaffold (Bemis & Murcko, 1996), a coarse representation of 2D molecular structure. Scaffold splits are commonly used to evaluate generalization of deep learning models in cheminformatics applications (Wu et al., 2018).

J. Annotation Consistency Continued

J.1. Isomorphic Distribution Results

Table 7. Ensemble Annotation Comparison: CV is coefficient of variation, CONS is annotation consensus, MAJ is agreement with majority annotation. Focus is on the isomorphic annotation distribution $P(\tilde{n}|f)$.

METRIC	ENTROPY ENS	STANDARD ENS
MEAN COS_{HUN}	0.667	0.669
CV COS_{HUN}	0.116	0.115
MEAN $\hat{H}(\tilde{n} f)$	0.373	0.347
CV $\hat{H}(\tilde{n} f)$	0.628	0.340
CONS $\arg \max_{\tilde{n}} P(\tilde{n} f)$	0.874	0.930
MAJ $\arg \max_{\tilde{n}} P(\tilde{n} f)$	0.970	0.982

The isomorphic distributions $P(\tilde{n}|f)$ have lower average normalized entropy than their counterparts $P_{\theta}(n|f)$. Intuitively this is because part of the entropy $\hat{H}_{\theta}(n|f)$ can be explained as distributing probability over subgraphs that are isomorphic. Note that the Entropy Ensemble still has twice the amount of entropy variation (in terms of CV $\hat{H}_{\theta}(\tilde{n}|f)$) than the Standard Ensemble, and lower CONS and MAJ metrics. These results are consistent with the analysis of the non-isomorphic distributions presented in Table 3.

J.2. Metric Definitions

Consider an ensemble of K models $P_{\theta}^{(1:K)} = \{P_{\theta}^{(1)}, \dots, P_{\theta}^{(K)}\}$. Let $\hat{F}(G, d, j) = \bigcup_{n \in V_{\mathcal{F}^d}} \{f_n^{-j}, \dots, f_n^j\}$ be the set of formulae derived from the approximate heavy-atom fragmentation DAG $G_{\mathcal{F}^d}$ with hydrogen tolerance j (similar to $\hat{M}(G, d, j)$ in Definition 4.3, but for formulae).

For molecule G_i in the dataset, the ensemble annotation consensus metric $\text{CONS } \arg \max_n P(n|f)$ is defined in Equation 21:

$$\begin{aligned} \text{CONS} \left(P_{\theta}^{(1:K)}, G_i, d, j \right) &= \frac{1}{|\hat{F}(G_i, d, j)|} \sum_{f_n \in \hat{F}(G_i, d, j)} \text{CONS} \left(P_{\theta}^{(1:K)}, f_n \right) \\ \text{CONS} \left(P_{\theta}^{(1:K)}, f_n \right) &= \mathbb{I} \left[\frac{K(K-1)}{2} = \sum_{k=1}^K \sum_{k'=k+1}^K \mathbb{I} \left[\arg \max_t P_{\theta}^{(k)}(t|f_n) = \arg \max_t P_{\theta}^{(k')}(t|f_n) \right] \right] \end{aligned} \quad (21)$$

The majority agreement metric MAJ $\arg \max_n P(n|f)$, which measures the fraction of models in the ensemble that agree with the most common annotation, is defined in Equation 22:

$$\begin{aligned} \text{MAJ} \left(P_{\theta}^{(1:K)}, G_i, d, j \right) &= \frac{1}{|\hat{F}(G_i, d, j)|} \sum_{f_n \in \hat{F}(G_i, d, j)} \text{MAJ} \left(P_{\theta}^{(1:K)}, f_n \right) \\ \text{MAJ} \left(P_{\theta}^{(1:K)}, f_n \right) &= \frac{1}{K} \sum_{k=1}^K \mathbb{I} \left[\arg \max_t P_{\theta}^{(k)}(t|f_n) = \text{mode}_{k'} \left(\arg \max_t P_{\theta}^{(k')}(t|f_n) \right) \right] \end{aligned} \quad (22)$$

In practice, instead of using the full formula set $\hat{F}(G_i, d, j)$, we restrict the set to formulae f_n that satisfy $\min_k P_{\theta}^{(k)}(f_n) \geq 0.05$.

K. Compound Retrieval Continued

Table 8. Compound Retrieval (Scaffold Split): Top- k Accuracy for different values of k , best scores are in bold.

MODEL	TOP-1 \uparrow	TOP-3 \uparrow	TOP-5 \uparrow	TOP-10 \uparrow
FRAGNNET-D4	21.1%	46.3%	60.0%	79.3%
FRAGNNET-D3	18.8%	43.9%	59.3%	77.8%
ICEBERG	18.3%	41.8%	55.0%	73.8%
MASSFORMER	10.1%	26.0%	39.5%	59.1%
NEIMS	10.2%	24.9%	35.9%	54.8%

The retrieval results on the Scaffold split are largely consistent with the results on the InChIKey split (Table 2), although the improvement of FraGNNNet-D4 over the other models is more pronounced. All models perform worse on the Scaffold split than they do on the InChIKey split, as expected.

L. Implementation Details

The FraGNNNet model and baselines were implemented in Python (Python Core Team 2021, version 3.10.13), using Pytorch (Paszke et al. 2019, version 2.1.0, CUDA 11.8) and Pytorch Lightning (Falcon & The PyTorch Lightning team 2019, version 2.1.2). Weights and Biases (Biewald 2020, version 0.16.1) was used to track model performance. The recursive fragmentation algorithm was implemented in Cython (Behnel et al. 2011, version 3.0.6). The graph neural network modules in FraGNNNet were implemented using Pytorch Geometric (Fey & Lenssen 2019, version 2.4.0). The data preprocessing and molecule featurization used RDKit (Landrum 2022, version 2022.09.4).

M. Parameter Counts

The parameter counts for the all of the models are summarized in Table 9. Note that ICEBERG-ADV has fewer parameters than ICEBERG since it does not use autoregressive fragment generation. The parameter counts for the binned models (MassFormer and NEIMS) are dominated by the weights for the final fully connected layer that maps to the 150,000 dimensional output spectrum. These approaches were originally designed for lower resolutions (0.1 Da binning), where the output spectrum has fewer bins.

Table 9. Parameter Counts: the -OUT entries for the binned models (NEIMS and MassFormer) correspond to counts which exclude the final projection into the output spectrum. Counts are reported in millions.

MODEL	# PARAMETERS
FRAGNNET-D4	1.6
FRAGNNET-D3	1.6
ICEBERG-ADV	3.5
ICEBERG	7.1
MASSFORMER	166.9
MASSFORMER (-OUT)	50.4
NEIMS	126.4
NEIMS (-OUT)	9.9

N. Baseline Model Implementation Details

All baseline models were re-implemented in our framework, to facilitate fair comparison across methods. Some of the models were originally designed to support additional covariates such as precursor adduct and instrument type: as our experiments were restricted to MS/MS data of a single precursor adduct ($[M+H]^+$) and instrument type (Orbitrap), we excluded these features in our implementations.

- NEIMS:** Neural Electron Ionization Mass Spectrometry (NEIMS, [Wei et al. 2019](#)) was the first deep learning C2MS model, originally designed for low resolution (1.0 Da bins) electron-ionization mass spectrometry (EI-MS) prediction. NEIMS represents the input molecule using a domain-specific featurization method called a molecular fingerprint, which capture useful properties of the molecule such as the presence or absence of various substructures. More recent works ([Zhu et al., 2020](#); [Young et al., 2023](#); [Goldman et al., 2023a](#)) have adapted NEIMS to ESI-MS/MS prediction at higher resolutions (0.1 Da bins). We based our implementation on the version from [Young et al. 2023](#) which uses three different kinds of molecular fingerprint representations: the Extended Connectivity (Morgan) fingerprint ([Rogers & Hahn, 2010](#)), the RDKit fingerprint ([Landrum, 2022](#)), and the Molecular Access Systems (MACCS) fingerprint ([Durant et al., 2002](#)). We adapted the model to use the same collision energy featurization strategy as FraGNNNet (Equation 19). Finally, to avoid an excess of parameters, we replaced the final fully-connected layer’s weight matrix with a low-rank approximation. This layer maps from the latent dimension $d_h = 1024$ to the output dimension $d_o = 150000$, corresponding to the mass range $[0, 1500]$ with 0.01 Da bins. The low-rank approximation was implemented as product of two learnable weight matrices: a $d_h \times d_r$ matrix and a $d_r \times d_o$ matrix, where $d_r = 256$.
- MassFormer:** The MassFormer model ([Young et al., 2023](#)) is a binned C2MS method originally designed for low resolution (1.0 Da bins) ESI-MS/MS prediction. It uses a graph transformer architecture ([Ying et al., 2021](#)) that is pre-trained on a large chemical dataset ([Nakata & Shimazaki, 2017](#)) and then fine-tuned on spectrum prediction. We preserved most aspects of the model’s original implementation but adapted the collision energy featurization and low rank output matrix approximation ($d_r = 128$) from the NEIMS baseline. Unlike the original MassFormer paper, we did not employ FLAG ([Kong et al., 2022](#)), a strategy for adversarial data augmentation in graphs, since none of the other models were using data augmentation.
- ICEBERG:** We describe the ICEBERG model ([Goldman et al., 2024](#)) in the main text (Section 5.1) and discuss it further in Appendix C. Our implementation is essentially unchanged from the original version, although in our experiments the model is trained using binned cosine similarity with 0.01 Da bins (previously, it was trained using 0.1 Da bins).